SERR Spectroelectrochemical Study of Cytochrome cd_1 Nitrite Reductase Co-Immobilized with Physiological Redox Partner Cytochrome c_{552} on Biocompatible Metal Electrodes

Célia M. Silveira[1,2]*, Pedro O. Quintas[1¤], Isabel Moura[2], José J. G. Moura[2], Peter Hildebrandt[3], M. Gabriela Almeida[2,4], Smilja Todorovic[1]*

1 Instituto de Tecnologia Química e Biológica, Universidade Nova de Lisboa, Oeiras, Portugal, 2 UCIBIO, REQUIMTE, Departamento de Química, Faculdade de Ciências e Tecnologia, Universidade Nova de Lisboa, Caparica, Portugal, 3 Technische Universitat Berlin, Institut fur Chemie, Berlin, Germany, 4 Centro de Investigação Interdisciplinar Egas Moniz (CiiEM), Instituto Superior de Ciências da Saúde Egas Moniz, Caparica, Portugal

¤ Current address: Department of Integrative Structural and Computational Biology and the Skaggs Institute for Chemical Biology, The Scripps Research Institute, La Jolla, California, United States of America
* c.silveira@fct.unl.pt (CMS); smilja@itqb.unl.pt (ST)

Abstract

Cytochrome cd1 nitrite reductases (cd_1NiRs) catalyze the one-electron reduction of nitrite to nitric oxide. Due to their catalytic reaction, cd_1NiRs are regarded as promising components for biosensing, bioremediation and biotechnological applications. Motivated by earlier findings that catalytic activity of cd_1NiR from *Marinobacter hydrocarbonoclasticus* (*Mhcd*$_1$) depends on the presence of its physiological redox partner, cytochrome c_{552} (cyt c_{552}), we show here a detailed surface enhanced resonance Raman characterization of *Mhcd*$_1$ and cyt c_{552} attached to biocompatible electrodes in conditions which allow direct electron transfer between the conducting support and immobilized proteins. *Mhcd*$_1$ and cyt c552 are co-immobilized on silver electrodes coated with self-assembled monolayers (SAMs) and the electrocatalytic activity of Ag // SAM // *Mhcd*$_1$ // cyt c_{552} and Ag // SAM // cyt c_{552} // *Mhcd*$_1$ constructs is tested in the presence of nitrite. Simultaneous evaluation of structural and thermodynamic properties of the immobilized proteins reveals that cyt c_{552} retains its native properties, while the redox potential of apparently intact *Mhcd*$_1$ undergoes a ~150 mV negative shift upon adsorption. Neither of the immobilization strategies results in an active *Mhcd*$_1$, reinforcing the idea that subtle and very specific interactions between *Mhcd*$_1$ and cyt c_{552} govern efficient intermolecular electron transfer and catalytic activity of *Mhcd*$_1$.

Introduction

Cytochrome cd_1 nitrite reductases (cd_1NiRs) are periplasmic proteins involved in the second step of the denitrification pathway ($NO_3^- \rightarrow \mathbf{NO_2^-} \rightarrow \mathbf{NO} \rightarrow N_2O \rightarrow N_2$), corresponding to the reduction of nitrite to nitric oxide [1–3]. cd_1NiRs are homodimeric proteins containing one c-type and one d_1-type heme per subunit. The heme c is thought to be the electron entry site, receiving electrons from small electron donor proteins, such as c-type cytochromes (cytochrome c_{552} [cyt c_{552}], cytochrome c_{551}, cytochrome c_{550}) or copper proteins (azurin, pseudoazurin); the electrons are then used for nitrite reduction by heme d_1 [1–3]. This cofactor is quite distinct from other types of hemes, due to its asymmetric porphyrin ring and a highly ruffled structure. So far heme d_1 has only been identified in cd_1NiR enzymes isolated from denitrifying bacterial species, e.g. *Marinobacter hydrocarbonoclasticus*, *Pseudomonas stutzeri*, *Pseudomonas aeruginosa* and *Paracoccus pantotrophus* [1,2,4]. The enzymes from the last two organisms have been thoroughly characterized, mainly by X-ray crystallography and fast kinetics. Unusual structural and catalytic features have been reported concerning, in particular, i) activation mechanisms, which involve redox driven structural changes, including conformational rearrangements and heme ligand exchange [5–7], and ii) the release of the reaction product NO from the active site, to avoid the formation of a dead-end product (i.e. Fe^{2+}-NO), since NO has a high affinity towards ferrous hemes [8–11]. Crystallographic structures of *P. pantotrophus* ($Ppcd_1$) and the *P. aeruginosa* ($Pacd_1$) cd_1NiRs reveal different cofactor coordination patterns in the oxidized states and similar catalytically competent reduced forms [6,12]; the information about structural and mechanistic properties of cd_1NiR from *M. hydrocarbonoclasticus* ($Mhcd_1$) is lagging behind.

Due to the reaction that they catalyze, cd_1NiRs are considered to be promising biocatalysts for the construction of electrochemical nitrite biosensors. These devices are expected to be able to selectively quantify nitrite in complex matrices and have broad applications, e.g. in drinking water regulation, environmental monitoring, clinical diagnosis and biomedical research [13,14]. A widely used approach for fabricating 3rd generation biosensors consists of the immobilization of the enzyme on an electrode that serves as a controllable electron source to drive the reaction cycle. The communication between the enzyme and the electrode relies on efficient direct electron transfer (ET), thereby increasing selectivity, simplifying the manufacturing process and reducing the number of components of the device. One of the major obstacles in the development of these devices is the immobilization of the enzyme in the native state, while maintaining good electrical contact with the transducer surface and ensuring high catalytic efficiency [15,16]. The electrochemical methods, which are typically used to monitor the performance of a biosensor, cannot provide information on the molecular origin of altered (or absent) catalytic or redox activity of the enzyme, which is often a consequence of immobilization induced structural changes. This can be overcome by coupling the electrochemical with spectroscopic methods, which give insights into the structural features of immobilized proteins [17,18]. In the case of cd_1NiRs, information on structural features of cofactors can be provided by resonance Raman (RR) spectroscopy that selectively probes redox, coordination and spin states of the heme groups upon excitation in resonance with their electronic transitions. When the protein is in close proximity to a nanostructured Ag surface, both plasmonic and resonance enhancements are matched using 413 nm excitation. Then the RR bands become further enhanced by several orders of magnitude (surface enhanced RR, SERR) allowing to probe the catalytic and/or redox site of the immobilized proteins only [19–21]. Moreover, a comparison of RR spectra in solution with SERR spectra of the adsorbed protein unambiguously reveals immobilization induced conformational alterations, if present.

Previous electrochemical studies of cd_1NiR showed that the enzyme is capable of nitrite reduction only in the presence of putative electron donor proteins. Using non-physiological redox mediators (e.g. yeast cyt c or ferricyanide) results in only residual electrocatalytic response [22,23]. Enzymatic activity could be measured with cd_1NiR and its physiological electron donor in solution, incorporated into polymeric films or entrapped with a dialysis membrane on the electrode surface [22–24]. However, despite all the efforts, including our own work, up to date there has been no report of direct ET between cd_1NiRs and electrode surfaces [22,23,25].

To further explore the potential use of $Mhcd_1$ for the development of nitrite biosensors, in this work we have searched for conditions which lead to a functional catalytic complex between $Mhcd_1$ and its physiological electron donor, cyt c_{552}. Direct contact of the proteins with the electrode surface, which can cause protein denaturation, was avoided by functionalization of the metal electrodes with alkanethiol based self-assembled monolayers (SAMs). SERR spectroelectrochemistry was employed to individually characterize $Mhcd_1$, cyt c_{552} and their complexes adsorbed on biocompatible metal electrodes and evaluate the impact of immobilization on the structural and thermodynamic properties of the proteins. Cyclic voltammetry was used to probe the catalytic activity of the immobilized $Mhcd_1$ in the presence/absence of cyt c_{552}. The obtained results shed light on the potential utilization of immobilized cd_1NiRs in bioelectrochemical devices for biotechnological applications.

Materials and Methods

Reagents and proteins

6-amino-1-hexanethiol hydrochloride and 11-amino-1-undecanethiol hydrochloride were purchased from Dojindo; all other chemicals were purchased from Sigma-Aldrich. The reagents were analytical grade and used without further purification. Solutions were prepared with deionized water (18MΩ.cm) from a Millipore MilliQ water purification system. $Mhcd_1$ (100 µM in 50 mM Tris-HCl buffer, pH 7.6, unless stated otherwise) and cyt c_{552} (150 µM in 50 mM Tris-HCl buffer, pH 8) were purified from $M.\ hydrocarbonoclasticus$ cells as previously described [26,27].

Electrode modification and protein immobilization

The nanostructured silver ring electrodes were prepared as previously described [28]. The roughened electrodes were subsequently coated with bifunctional alkanethiol-based SAMs by immersion into 1 mM ethanolic solution of the monolayer. The following pure and mixed SAMs were used: ethanethiol, 1-propanethiol, 1-hexanethiol, 1-undecanethiol, 2-mercaptoethylamine hydrochloride, 6-amino-1-hexanethiol hydrochloride, 11-amino-1-undecanethiol hydrochloride, 6-mercaptohexanoic acid, 11-mercaptoundecanoic acid, 6-mercapto-1-hexanol and 11-mercapto-1-undecanol. The proteins were adsorbed on the SAM-coated electrodes following two different procedures: the modified electrode was i) immersed for 1 hour in a 0.1 µM protein solution (in supporting electrolyte, 12.5 mM potassium phosphate, 12.5 mM K_2SO_4, pH 7), then removed and rinsed with supporting electrolyte to eliminate unbound or loosely bound protein or ii) directly placed into the SERR spectroelectrochemical cell containing the supporting electrolyte and 0.1 µM protein, which was allowed to adsorb at open circuit for 30 min; additionally, positive or negative potentials were applied to the electrode during "in-cell" adsorption. The protein-containing solution was afterwards replaced by a protein-free supporting electrolyte. The duration of the immobilization procedure, protein concentration, pH of the buffer and temperature were previously optimized.

SERR spectroelectrochemistry

The potential-controlled SERR experiments were performed using a home-built spectroelectrochemical cell equipped with an Ag/AgCl (3 M, KCl) reference electrode (210 mV vs. the standard hydrogen electrode, SHE) and a platinum wire counter electrode. The experiments were carried out in 12.5 mM potassium phosphate and 12.5 mM K_2SO_4, pH 7, except for nitrite activity assays, where 50 mM MES buffer with 50 mM KCl, pH 6.3 was used. A confocal microscope, equipped with an Olympus 20X objective (working distance of 21 mm, numeric aperture of 0.35), was used for laser focusing onto the sample and light collection in the back-scattering geometry. The microscope was coupled to a Raman spectrometer (Jobin Yvon U1000), equipped with a 1200 lines/mm grating and a liquid nitrogen-cooled CCD detector. The 413 nm line from a krypton ion laser (Coherent Innova 302) was used as the excitation source. The laser beam was focused onto the surface of the enzyme modified electrode with a power of ca. 1.5 – 2.5 mW; spectral accumulation time was typically 30 s; 3 – 5 spectra were co-added in each measurement to improve signal to noise (S/N) ratio. The working electrode was kept under constant rotation (600 rpm). The electrode potentials were controlled using a Princeton Applied Research 263A potentiostat. All spectra were subjected to polynomial baseline subtraction; the positions and widths of Raman bands were determined by component analysis as described previously [29]. Redox parameters of $Mhcd_1$ were obtained by fitting the normalized intensity of the ν_4 band of the measured, potential dependent SERR spectra to the Nernst equation; in the case of cyt c_{552} the SERR spectra were subjected to a component analysis taking into account the ν_4, ν_3, ν_2 and ν_{10} modes, the redox parameters were then estimated from fits of the relative concentrations of the oxidized and reduced species plotted as a function of the electrode potential [29].

Cyclic voltammetry experiments were performed in the SERR spectroelectrochemical cell. The supporting electrolyte solution was thoroughly deoxygenated using oxygen-free argon prior to electrochemical measurements. To evaluate the response of the bioelectrode constructs to nitrite, small volumes of sodium nitrite solutions were successively added to the cell.

All potentials are quoted versus SHE.

RR spectroscopy

The RR spectra were measured with 413 nm excitation (*vide supra*) in a rotating cuvette (Hellma) filled with ca. 80 μL of sample. Protein concentration was 100 and 150 μM for $Mhcd_1$ and cyt c_{552}, respectively. The laser power and accumulation time were 1.5 – 3.5 mW and 20 – 40 s; typically 3 – 10 spectra were co-added in each measurement to improve S/N. The spectra were submitted to component analysis as described in the previous section.

RR potentiometric titrations: The $Mhcd_1$ samples were prepared in a N_2 atmosphere, inside an anaerobic chamber ($O_2 < 2$ ppm). Step-wise reduction of the ferric enzyme was achieved by addition of small volumes of sodium dithionite solution (1 mM, Tris-HCl 100 mM, pH 7.6); at each point the solution potential was measured with a combined platinum—Ag/AgCl electrode (207 mV vs. SHE). Upon each addition of the reductant, the RR cell was removed from the glove box and the spectra were measured; a fresh aliquot of protein was used for each measurement (i.e. each data point in the titration curve). The protein concentration was 60 μM in a Tris-HCl 50 mM, pH 7.6 buffer containing a mixture of redox mediators at 10 μM each: 1,2-naphthoquinone-4-sulfonic acid (215 mV), 1,2-naphthoquinone (180 mV), trimethylhydroquinone (115 mV), phenazine methosulfonate (80 mV), methylene blue (11 mV), resorufin (−51 mV), indigo disulfonate, (−125 mV), 2-hydroxy-1,4-naphthoquinone (−145 mV), anthraquinone-2-sulfonic acid (−182 mV) and phenosafranine (−255 mV). Redox parameters were obtained as described in previous sections.

Binding of NO to $Mhcd_1$: Protein concentration was 75 μM in 50 mM Tris-HCl, pH 7.6. The solutions of either resting ferric state, or ferrous $Mhcd_1$, were first degassed with argon (reduction of the ferric enzyme was achieved by addition of sodium dithionite or sodium ascorbate). The $Mhcd_1$-NO adducts were prepared inside an anaerobic chamber by the addition of a NO releasing compound (diethylamine NONOate in 10 mM NaOH) to the cell completely filled with the protein solution (10 times the protein concentration). At the pH at which the experiments were performed, each diethylamine NONOate molecule releases 1.5 molecules of NO (t½ = 16 min, at 25°C, pH 7.4). The RR cell was then tightly closed with thick Teflon stoppers which do not allow oxygen diffusion into the cell during RR measurements. The spectra of the ferric and ferrous protein samples were also acquired immediately prior to the addition of diethylamine NONOate.

UV-Vis spectroscopy

UV-Vis absorption spectra were recorded using a Shimadzu UV-1203 spectrophotometer. The samples were prepared in quartz cuvettes with a path length of 10 mm, sealed with silicone septa. All measurements were performed at room temperature. Protein concentration was 5 μM in Tris-HCl 50 mM, pH 7.6 buffer. The ferric and ferrous NO adducts were prepared as described in the previous section. All measurements were performed inside an anaerobic chamber ($O_2 < 2$ ppm).

Results and Discussion

Our earlier findings revealed that the catalysis of $Mhcd_1$ depends on the presence of its physiological redox partner, cyt c_{552} [23,24]. We have therefore focused on the formation and characterization of a functional catalytic complex between $Mhcd_1$ and cyt c_{552}.

Co-immobilization of cyt c_{552} and $Mhcd_1$

Co-immobilization of cyt c_{552} and $Mhcd_1$ was achieved by sequential incubation of SAM-coated silver electrodes with the two proteins, cyt c_{552} followed by cd_1NiR and vice versa, resulting in the following constructs: Ag // SAM // cyt c_{552} // $Mhcd_1$ and Ag // SAM // $Mhcd_1$ // cyt c_{552}. For each case, several alkanethiol-based SAMs (e.g. NH_2^+-, CH_3-, COO^--and OH-terminated) and their mixtures in different molar ratios were tested. The SERR signal intensities of cyt c_{552} were optimized on surfaces coated with 6-mercapto-1-hexanol/1-hexanethiol (OH/CH_3) and of $Mhcd_1$ on 11-amino-1-undecanethiol hydrochloride/1-undecanethiol (NH_2^+/CH_3) in 1:1 molar ratios; the former confers mostly polar-hydrophobic surface for cyt c_{552} adsorption, and the latter positively charged-hydrophobic surface for $Mhcd_1$ attachment. These SAMs provided ca. 2 to 3 times stronger signals of cyt c_{552} and $Mhcd_1$, respectively, than the other tested monolayers. Successful co-immobilization of the two proteins on the same electrode construct was demonstrated by SERR (Fig 1), based on individual spectroscopic fingerprints of the ferric and ferrous cyt c_{552} and $Mhcd_1$, which could be identified in the SERR spectra of the complex. Spectral parameters, e.g. band frequencies and widths (Table 1), which were used to deconvolute the SERR spectra of the cyt $c_{552}/Mhcd_1$ complexes were derived from RR spectra (Fig 2, traces a and c).

Characteristic RR marker bands: ν_4, ν_3, ν_2 and ν_{10} of the His/Met coordinated cyt c_{552} are found at 1375, 1508, 1587 and 1641 cm^{-1}, respectively, for the ferric and at 1364, 1497, 1592 and 1627 cm^{-1}, respectively, for the ferrous protein in solution, indicating a six-coordinated low spin heme (6cLS) configuration (Fig 2A, Table 1) [30,31]. The spectra are comparable with those of cytochrome c_{551} from $P.$ $aeruginosa$, measured with 413 nm excitation, and reveal small but systematic frequency upshifts [32]. A comparison of RR spectra of ferric and ferrous
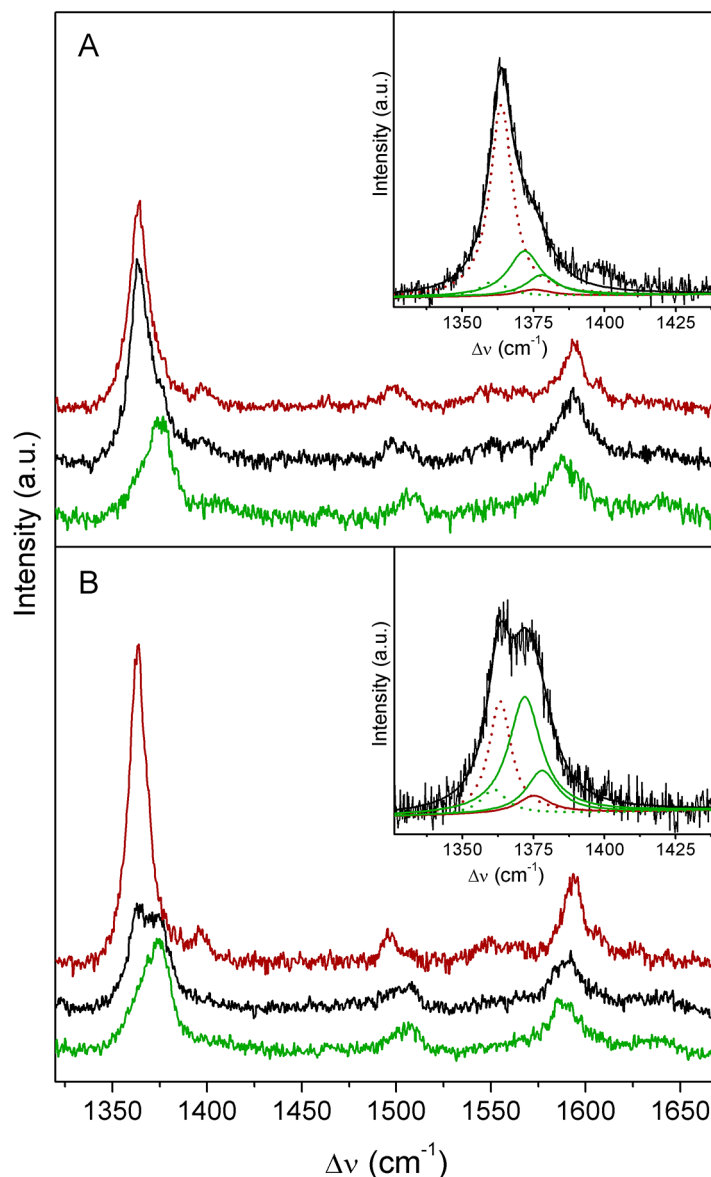
Fig 1. SERR spectra of co-immobilized *Mhcd$_1$* and cyt *c$_{552}$*. A) Ag // 6-mercapto-1-hexanol/1-hexanethiol // cyt *c$_{552}$* // *Mhcd$_1$* and **B)** Ag // 11-amino-1-undecanethiol hydrochloride/1-undecanethiol // *Mhcd$_1$* // cyt *c$_{552}$* constructs at different poised potentials: 300 mV (green), 200 mV (black) and 0 mV (red). **Inset:** component analysis of experimental spectra (black traces) in ν_4 region of co-adsorbed *Mhcd$_1$* and cyt *c$_{552}$* measured at 200 mV; cyt *c$_{552}$* (red) and *Mhcd$_1$* (green) populations; overall fit (black). Solid traces designate ferric and dotted traces ferrous ν_4 components. The spectra were recorded with 413 nm excitation; laser power and accumulation time were 1.5 mW and 30 s, respectively.

cyt c_{552} in solution with SERR spectra of adsorbed cyt c_{552} at positive (400 mV) and negative (−100 mV) potential indicates that the native protein structure is preserved upon immobilization on OH/CH$_3$ SAMs (Fig 2A, Table 1). The absence of band broadening also indicates that the orientation of immobilized cyt c_{552} was uniform. Note that, under the experimental conditions used in this work, the positive potentials required to achieve complete cyt c_{552} reduction (400 mV) did not cause the oxidation of the Ag electrode.

Table 1. Frequencies of RR and SERR marker bands of $Mhcd_1$ and cyt c_{552}.

	ν_i ($\Delta\nu$)/ cm^{-1}	ν_4	ν_3	ν_2	ν_{10}
RR	Ferric $Mhcd_1$	1372 (11.0); 1378 (13.5)	1505 (11.5)	1585 (14.8)	1637 (10.3)
	Ferrous $Mhcd_1$	1362 (9)	1494 (8.5)	1589 (14.1)	1623 (9.3)
	Ferric $Mhcd_1$-NO	[a] 1362	1494	1582	1624
		[b] 1370	1503	1587	1635
		[c] 1377	-	1592	1640
	Ferrous $Mhcd_1$-NO	1363	1492	1582	1624
		[b] 1370	1503	1587	1634
		[c] 1378	-	1593	1640
SERR	Ferric $Mhcd_1$	1372 (13); 1378 (13.5)	1505 (12.8); 1511 (11.9)	1588 (14.4)	1639 (11.5)
	Ferrous $Mhcd_1$	1361 (10.9)	1493 (10)	1593 (14)	1624 (9)
RR	Ferric cyt c_{552}	1375 (14.1)	1508 (11.5)	1587 (13.4)	1641 (8.6)
	Ferrous cyt c_{552}	1364 (10.3)	1497 (9.0)	1592 (13.9)	1627 (8.3)
SERR	Ferric cyt c_{552}	1375 (14.1)	1507 (11.5)	1586 (13.4)	1640 (8.6)
	Ferrous cyt c_{552}	1363 (10.7)	1496 (9.2)	1593 (13.9)	1626 (7.5)

Assignment of marker bands (ν_i) of $Mhcd_1$ and cyt c_{552} in the ferric and ferrous states determined from the RR and SERR spectra recorded with 413 nm excitation. SERR spectra were measured from SAM-coated Ag electrodes, with cyt c_{552} immobilized on 6-mercapto-1-hexanol/1-hexanethiol; ferric and ferrous states were obtained at electrode potentials of 400 mV and −100 mV, respectively, and $Mhcd_1$ immobilized on 11-amino-1-undecanethiol hydrochloride/1-undecanethiol; ferric and ferrous states were obtained at electrode potentials of 300 mV and −300 mV, respectively. For the $Mhcd_1$-NO adducts the vibrational modes of the three identified populations, auto-reduced $Mhcd_1$, 6cLS and 5cHS d_1, are presented. The bandwidths ($\Delta\nu$) used for quantitative component analysis are given in parenthesis.
[a]Auto-reduced in ferric protein (c^{2+}).
[b]Ferrous 6cLS NO adduct (c^{2+}/6cLS d_1^{2+}-NO).
[c]Ferrous 5cHS NO adduct (c^{2+}/5cHS d_1^{2+}-NO).

doi:10.1371/journal.pone.0129940.t001

The RR marker bands of $Mhcd_1$ (ν_4, ν_3, ν_2 and ν_{10} at 1372 cm^{-1}, 1505 cm^{-1}, 1585 and 1637 cm^{-1} in the ferric and at 1362, 1494, 1589 and 1623 cm^{-1} in the ferrous state, respectively) suggest the presence of the 6cLS heme state. SERR spectra of the immobilized enzyme measured at the positive (300 mV) and negative (−300 mV) potentials show minor shifts in comparison with those observed in RR spectra (Fig 2B, Table 1). Under equivalent experimental conditions, RR spectra of ferrous $Pacd_1$ reveal a consistent band upshift (ν_4, ν_3 and ν_2 at 1368 cm^{-1}, 1500 cm^{-1} and 1597 cm^{-1}) [33]. It is noteworthy that in some cases, we observe a shoulder at 1362 cm^{-1} on the ferric ν_4 band, indicative of laser induced photo-reduction; this population increases proportionally to the laser power and accumulation time. Its contribution in the spectra was kept as low as possible by using a compromise between a reasonable S/N ratio and minimal photo-reduction.

Albeit small, differences in the frequencies of the marker bands between cyt c_{552} and $Mhcd_1$ allow for a complete separation of their SERR spectral contributions when they are simultaneously present on the electrode (Fig 1A and 1B). The presence of the two proteins becomes especially evident upon applying potentials in the 0 − 200 mV range, at which $Mhcd_1$ is almost or fully oxidized and cyt c_{552} nearly or fully reduced (Fig 1, red and black traces). Component analysis of the ν_4 mode region measured at 200 mV on Ag // OH/CH$_3$ // cyt c_{552} // $Mhcd_1$ (Fig 1A, inset) and on Ag // NH$_2^+$/CH$_3$ // $Mhcd_1$ // cyt c_{552} (Fig 1B, inset), further reinforces evidence for the presence of the two proteins on the same electrode construct. At electrode potential of 200 mV, the SERR spectrum of Ag // OH/CH$_3$ // cyt c_{552} // $Mhcd_1$ complex is dominated
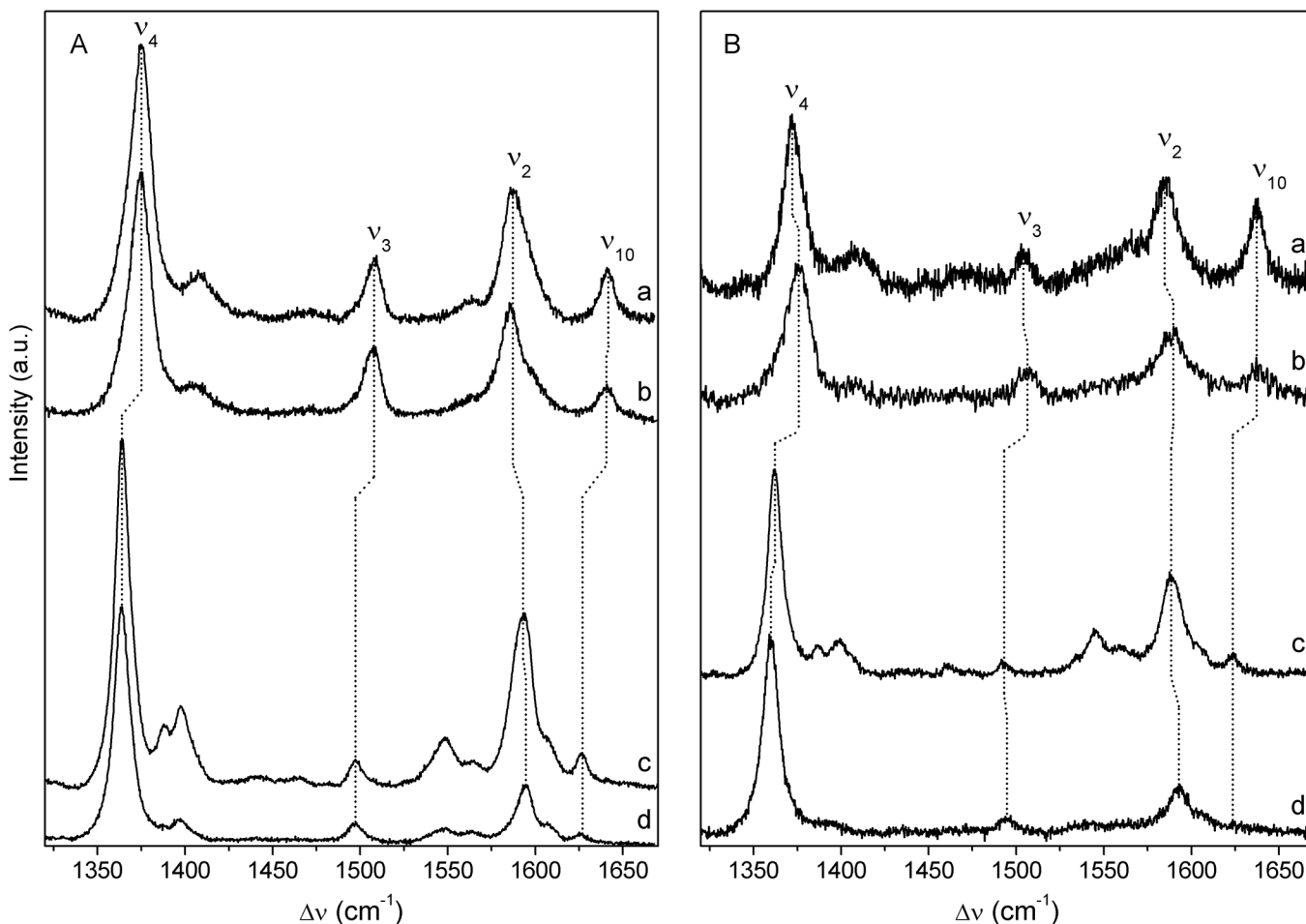
Fig 2. RR and SERR spectra of cyt c_{552} and $Mhcd_1$. A) cyt c_{552}: RR spectra of (a) ferric and (c) sodium ascorbate reduced, ferrous protein; SERR spectra of cyt c_{552} immobilized on 6-mercapto-1-hexanol/1-hexanethiol SAM at electrode potentials of (b) 400 mV and (d) –100 mV. **B)** $Mhcd_1$: RR spectra of (a) ferric and (c) sodium ascorbate reduced, ferrous enzyme; SERR spectra of $Mhcd_1$ on 11-amino-1-undecanethiol hydrochloride/1-undecanethiol SAM at electrode potentials of (b) 300 mV and (d) –300 mV. The spectra were recorded with 413 nm excitation; laser power and accumulation time were 2 – 3 mW and 40 s (RR) or 1.5 – 2.5 mW and 30 s (SERR).

by the features of cyt c_{552} (Fig 1A, black trace and inset) due to a greater plasmonic enhancement, resultant of the closer proximity of cyt c_{552} to the nanostructured metal. In addition, cyt c_{552} is already fully reduced at this potential (ν_4 at 1364 cm^{-1}), at which $Mhcd_1$ is largely oxidized (ν_4 at 1372 cm^{-1}). Similarly, at 300 mV (Fig 1A, green trace) and 0 mV (Fig 1A, red trace), SERR spectra are dominated by the fully oxidized and reduced cyt c_{552}, respectively. In Ag // NH$_2^+$/CH$_3$ // $Mhcd_1$ // cyt c_{552} constructs, in which $Mhcd_1$ is adsorbed to the electrode prior to cyt c_{552}, its contribution in the spectra becomes more evident (Fig 1B). At 200 mV (Fig 1B, black trace and inset), the SERR signal is composed of nearly equal contributions from the two proteins, predominantly ferrous cyt c_{552} (Fig 1B, inset, dotted red trace) and ferric $Mhcd_1$ (Fig 1B, inset, solid green traces). Notably, the SERR signal of the two proteins is sufficiently strong even for thick spacers (e.g. 1-undecanethiol, eleven CH$_2$ groups).

Despite a direct spectroscopic evidence that $Mhcd_1$ and cyt c_{552} were simultaneously attached to the electrode surface, none of the tested conditions led to catalytically active $Mhcd_1$, as no catalytic currents were detected in the presence of nitrite (S1 Fig). In the next approach Ag // NH$_2^+$/CH$_3$ // $Mhcd_1$ + solution cyt c_{552} and Ag // NH$_2^+$/CH$_3$ // cyt c_{552} + solution $Mhcd_1$
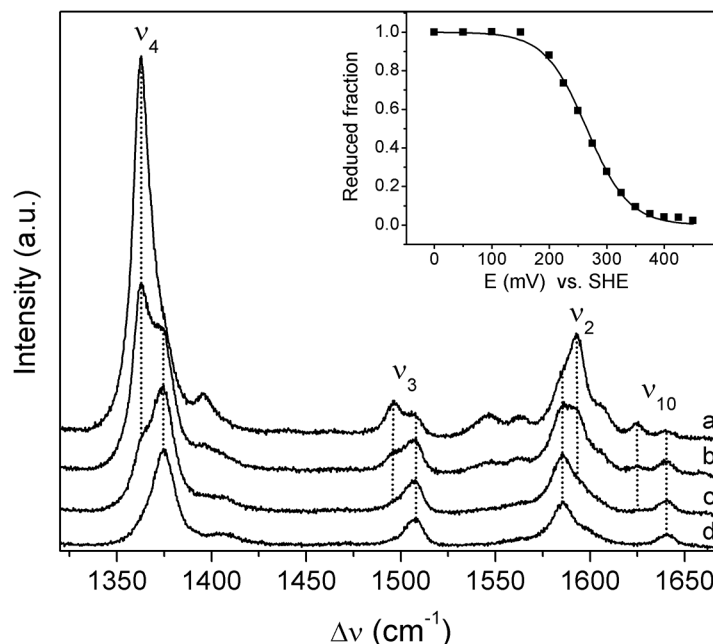
Fig 3. Potentiometric titration of immobilized cyt c_{552}. SERR spectra of cyt c_{552} immobilized on 6-mercapto-1-hexanol/1-hexanethiol SAM-coated Ag electrode recorded at electrode potentials of (a) to (d) 250, 300, 350 and 450 mV. All spectra were measured with 413 nm excitation; laser power and accumulation time were 1.5 mW and 30 s, respectively. **Inset:** relative concentration of ferrous protein (squares) plotted as a function of the electrode potential. The solid line represents a fit of the experimental data to the Nernst equation, yielding $E°' = 262 ± 5$ mV, $z = 0.70 ± 0.02$.

constructs were created, in which one of the proteins was immobilized on the electrode surface and the other was confined in its proximity by securing a dialysis membrane around the electrode body. Thus, the partner protein was free to orientate and dock to the immobilized redox partner. Electrocatalytic activity of $Mhcd_1$ was not measurable under either of these conditions.

In order to understand the reasons for the lack of catalytic activity of $Mhcd_1$ co-immobilized with cyt c_{552}, in the next step we probed the thermodynamic (i.e. redox potential, $E°'$) properties of immobilized cyt c_{552} and $Mhcd_1$ in Ag // OH/CH₃ // cyt c_{552} and Ag // NH₂⁺/CH₃ // $Mhcd_1$ constructs respectively, and compared them with the respective features of the two proteins in solution.

Cyt c_{552} immobilized on biocompatible electrodes

First, the redox potential of the immobilized cyt c_{552} was determined by electrochemical redox titrations followed by SERR spectroscopy (Fig 3). The component analysis of the potential dependent SERR spectra of cyt c_{552} in which ν_4, ν_3, ν_2 and ν_{10} modes were considered, provides the relative spectral contributions of the ferric and ferrous heme c. The spectral parameters (e.g. frequencies and band widths) of each vibrational mode, defined in RR spectra of ferric and ferrous protein, were kept constant such that the only variables at a given potential are the amplitudes of the individual component spectra. The apparent redox potential was estimated from fits to the relative concentrations of the oxidized and reduced species plotted as a function of the electrode potential. The Nernst plot (Fig 3, inset) reveals a redox transition at $E°' = 262 ± 5$ mV and an apparent number of transferred electrons, z, of $z = 0.70 ± 0.02$ for the immobilized cyt c_{552}, which is in good agreement with UV-Vis potentiometric titrations of the

protein in solution (~ 260 mV) [30]. Additionally, the SERR electrode constructs (Ag // OH/ CH₃ // cyt c_{552}) were characterized by cyclic voltammetry (S2 Fig); cyt c_{552} displayed one-electron quasi-reversible electrochemistry, with peak separations up to 50 mV in the studied scan rate range (0.01 to 0.5 V s⁻¹) and widths at half height around 130 mV. The peak currents varied linearly with the scan rate in the whole range tested, thus demonstrating that cyt c_{552} was adsorbed on the surface of the modified electrode. The $E°'$ (249 ± 2 mV) was determined by the average of anodic and cathodic peak potentials; it was independent of the scan rate and comparable with the value derived from the spectroscopic experiments. Taken together, these results demonstrate that cyt c_{552} retains its redox properties and native structure (*vide supra*) upon immobilization on OH/CH₃ SAM-coated silver electrodes.

$Mhcd_1$ immobilized on biocompatible electrodes

The analysis of the redox behavior of the immobilized $Mhcd_1$ is not as straightforward, due to i) possible ambiguities related to the presence of two hemes and ii) the presence of more than one spin species, particularly evident upon component analysis of the RR and SERR spectra of the ferric protein (cf. Table 1). Although the high frequency region of the RR spectra of the resting state $Mhcd_1$ (Fig 2B), obtained with 413 nm excitation, reveals features characteristic of *c*-type heme proteins, in principle, contributions from both hemes, *c* and d_1, could be expected since their respective Soret bands coincide in the ferric enzyme (S3 Fig, trace a). However, a comparison of the extinction coefficients for the ferric isolated d_1 cofactor (30.5 mM⁻¹.cm⁻¹) and His/Met (105 mM⁻¹.cm⁻¹) or His/His (97.5 mM⁻¹.cm⁻¹) coordinated *c* hemes [34,35], found in cd_1NiRs from *P. aeruginosa* ($Pacd_1$) and *P. pantotrophus* ($Ppcd_1$), respectively, indicates that the resonance enhancement and therefore the spectral contribution of heme d_1 should be considerably lower than that of heme *c*. In the reduced enzyme, heme *c* is selectively enhanced with 413 nm excitation [33] since the low intensity Soret band of the ferrous heme d_1 is further red-shifted to 460 nm (S3 Fig, trace d). Therefore, we attribute spectra of ferric and ferrous enzyme measured with 413 nm to heme *c* of $Mhcd_1$.

Deconvolution of SERR spectra of the oxidized $Mhcd_1$ immobilized on NH₂⁺/CH₃ SAMs and measured at potentials $\geq$ 200 mV, reveals that the ν_4 mode is composed of two ferric components, centered at 1372 cm⁻¹ and 1378 cm⁻¹. Likewise, the component analysis of the RR spectra of $Mhcd_1$ in the resting state indicates that in the majority of cases the ν_4 mode has an additional component at 1378 cm⁻¹, which depending on the protein fraction, accounts for up to 15% of the ν_4 intensity (Fig 4A and 4B, blue trace; Table 1). We attribute the 1372 cm⁻¹ band to the native form, as it is largely dominant in solution, and the 1378 cm⁻¹ component to a non-native population and designate them as ox₁ and ox₂, respectively. In the spectra of immobilized $Mhcd_1$ (Fig 4B), we observe approx. 1:1 mixture of native and non-native populations. Both ox₁ and ox₂ are in 6cLS state, as revealed by the frequency of the broadened ν_3 mode ($\Delta\nu_3$ (SERR) = 17 cm⁻¹, $\Delta\nu_3$ (RR) = 11 cm⁻¹, Table 1), possibly representing two populations carrying different axial ligands. The SERR spectrum of the enzyme recorded at negative potential ($\leq$ −300 mV, Fig 4D) is indicative of the native ferrous enzyme (red₁) identified in the RR spectra of the ascorbate-reduced enzyme in solution (Fig 4C). After prolonged exposure of the enzyme to negative potentials and laser beam, a second non-native component of ferrous $Mhcd_1$ (ν_4 at 1355 cm⁻¹) could be identified in SERR spectra (Fig 4D). Note a slight broadening (1 – 2 cm⁻¹) of some SERR bands relative to those observed in RR spectra (Table 1), which is most likely related to orientation heterogeneity of the immobilized $Mhcd_1$ molecules.

In the next step, we probed the redox behavior of $Mhcd_1$ attached to NH₂⁺/CH₃ coated electrodes employing potential-dependent SERR spectroscopy. The SERR spectra, measured in the potential range between −400 and 350 mV (Fig 4E), were subjected to a component analysis, as
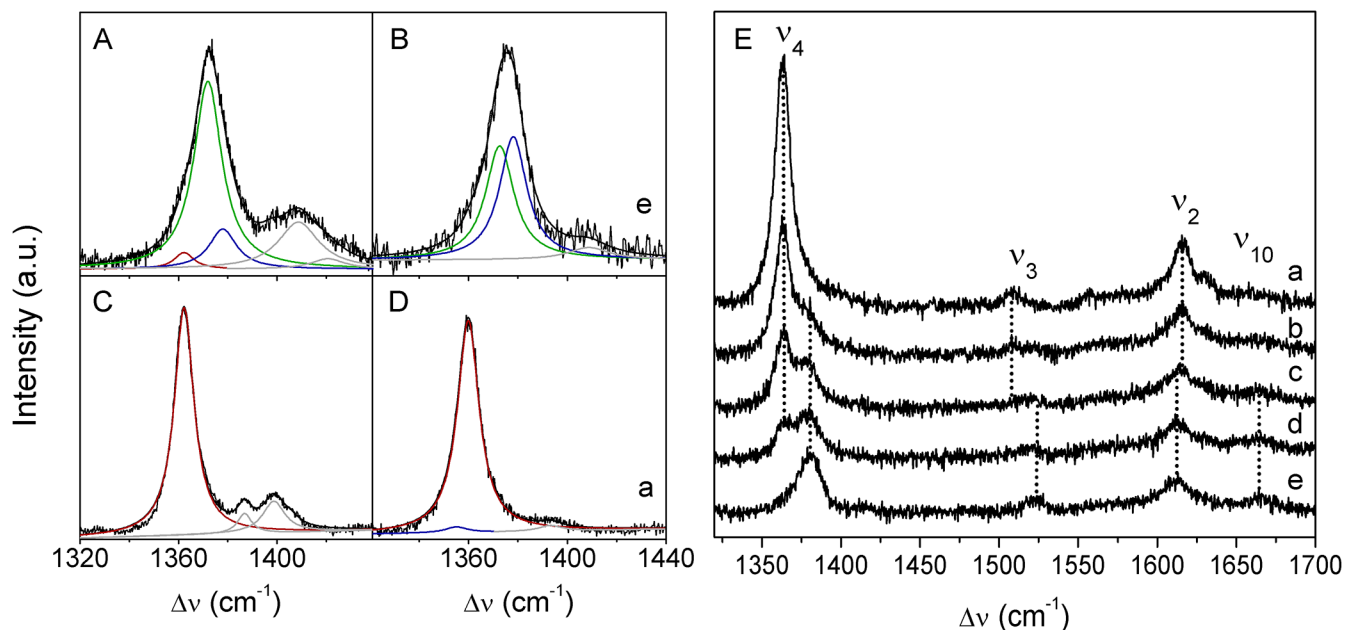
Fig 4. RR and SERR spectra of *Mhcd*$_1$. Component analysis of the ν_4 region of: RR spectra of **A)** ferric and **C)** ferrous *Mhcd*$_1$ and SERR spectra of *Mhcd*$_1$ immobilized on a 11-amino-1-undecanethiol hydrochloride/1-undecanethiol SAM at electrode potentials of **B)** 300 mV and **D)** –300 mV; green and red solid lines represent native ferric and ferrous populations, respectively, blue line accounts for non-native populations; gray line for non-assigned bands and black line for the overall fit. Red line in panel A indicates traces of photo-reduced protein. **E)** SERR spectra of *Mhcd*$_1$ recorded as a function of the electrode potential, from (a) to (e) –150, –50, 50, 100 and 300 mV. The spectra were recorded with 413 nm excitation; laser power and accumulation time were 3 mW and 40 s (RR) or 2.5 mW and 30 s (SERR), respectively.

doi:10.1371/journal.pone.0129940.g004

described for cyt c_{552} (*vide supra*). In the case of *Mhcd*$_1$ only ν_4 modes were considered, due to a poorer quality of the spectra. At each electrode potential, the spectra could be consistently analyzed on the basis of the two ferric (ox_1 and ox_2) and one ferrous (red_1) components. Also, relative intensities (I_i) were used in the analysis instead of relative concentrations (c_i), $c_i = f_i I_i$; this is a frequently adopted strategy when the factors f_i, that are proportional to the relative reciprocal SERR cross sections of the species i, are unknown [20]. The apparent redox potentials were estimated from fits to the relative band intensities plotted as a function of the electrode potential (Fig 5A). The Nernst plots reveal a redox transition at $E^{\circ\prime} \sim 70$ mV for the native redox couple (ox_1/red_1) of the immobilized *Mhcd*$_1$, which is assigned to heme *c*. The non-native population, as estimated from the potential-dependent contributions of ox_2, shows a much broader transition at $E^{\circ\prime} \sim 60$ mV.

In parallel, the reduction potential of *Mhcd*$_1$ was determined in solution by potentiometric titrations of the enzyme monitored by RR spectroscopy (Fig 5B). The spectra were recorded after a stepwise addition of sodium dithionite to the buffer containing the oxidized enzyme and a cocktail of redox mediators. The relative amounts of the reduced and oxidized populations were determined from the component analysis of ν_4 (Fig 5B, inset) at each solution potential. As described for the analysis of the SERR spectra, the ν_4 was fitted with two oxidized (ox_1 and ox_2) and one reduced (red_1) components. The relative amount of red_1 species plotted against the solution potential, shows a redox transition at $E^{\circ\prime} = 220 \pm 5$ mV and $z = 0.9 \pm 0.1$. The determined redox potential is in agreement with previous data from UV-Vis titrations of *Mhcd*$_1$ which suggested $E^{\circ\prime}$ (*c*) = 234 mV (and $E^{\circ\prime}$ (*d*$_1$) = 200 mV) [26]. Besides, this value is comparable with the redox potential of *Pacd*$_1$ ($E^{\circ\prime}$ (*c*, *d*$_1$) ~ 280 mV) and to that of *Ppcd*$_1$ semi-apoprotein ($E^{\circ\prime}$ (*c*) = 242 mV) [36,37].
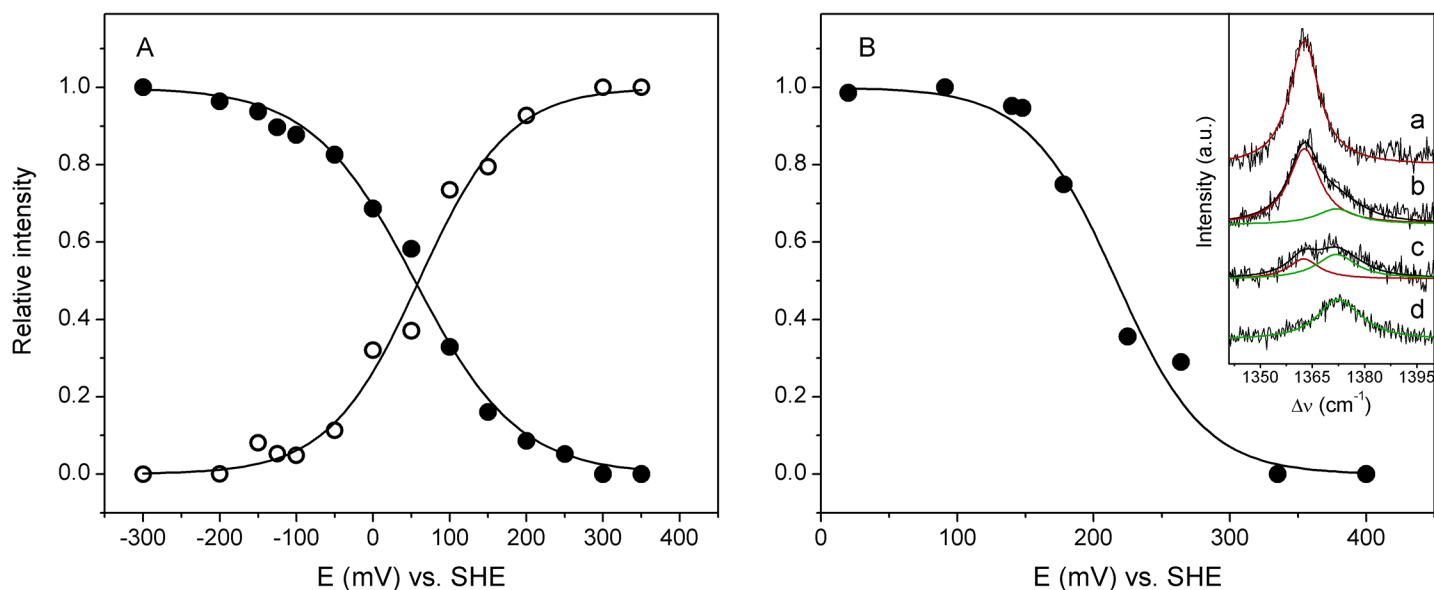
Fig 5. Redox titrations of $Mhcd_1$ in immobilized and solution state. A) SERR spectroelectrochemical titration of $Mhcd_1$ adsorbed on 11-amino-1-undecanethiol hydrochloride/1-undecanethiol coated electrodes. Data points correspond to the relative intensities of ferrous (ν_4 at 1362 cm^{-1}; solid circles) and ferric (ν_4 at 1372 cm^{-1}; open circles) heme c populations, as a function of the electrode potential. Solid lines represent fits of the Nernst equation, $E°' \sim 70$ mV, $z = 0.44$, to the experimental data points. **B)** RR redox titration of $Mhcd_1$ in solution. The relative intensities of the reduced population are represented as a function of the solution potential, solid circles. The Nernst equation was fitted to the data (black line) with $E°' = 220 \pm 5$ mV, $z = 0.90$. **Inset:** ν_4 band of RR spectra measured at solution potentials of (a) 90, (b) 180, (c) 225 and (d) 335 mV. Component spectra represent ferrous (red) and ferric (green) ν_4 populations and overall fit (black). The spectra were recorded with 413 nm excitation, with 2 – 3 mW laser power and 40 s accumulation time. **Note:** Sample preparation for solution RR titrations was performed in anaerobic conditions (glove box). Upon each addition of the reductant, the RR cell was removed from the glove box and the spectra were measured; a fresh aliquot of protein was used for each data point.

doi:10.1371/journal.pone.0129940.g005

A comparison of SERR and RR titrations shows that the redox transition in immobilized $Mhcd_1$ is ~150 mV lower than the value determined from the solution studies. Also, the number of transferred electrons in SERR titrations was consistently below 0.5, indicating that the electronic coupling of the protein's redox centers with the metal surface was not efficient. We associate the redox potential shift of the "native" portion of heme c in $Mhcd_1$ with immobilization induced conformational changes of the secondary structure that can significantly alter hydrophobicity of the heme pocket. While we can exclude major structural perturbations that influence the spin and coordination state of the heme c, they cannot be ruled out in the case of heme d_1, which could not be individually probed in the present work. According to Kassner's relation, opening of the cavity of heme c to the solvent and an increased polarity of the heme environment can result in a downshift of redox potentials of up to 0.2 V [38], which is consistent with the shift observed here. cd_1NiRs are actually prone to structural alterations, as a part of catalytic activation. For example, as demonstrated by X-ray crystallography, redox linked conformational changes in $Ppcd_1$ lead to a loss of hydrophobic interactions and hydrogen bond breakage between the domains harboring hemes c and d_1, resulting in increased water exposure of the interface between the two domains [12].

We further tested if the immobilized $Mhcd_1$ was capable of NO binding. The UV-Vis spectra of ferric and ferrous $Mhcd_1$, recorded upon addition of NO-releasing diethylamine NONOate, indicate that NO binds to the heme d_1 of both forms, as judged by the spectral changes, e.g. Soret band intensity increase, suggesting a blue shift of the 460 nm band of the ferrous d_1 (S3 Fig, trace c) and appearance of an additional band at 644 nm, characteristic of the NO bound 6sLS d_1 heme (S3 Fig, inset traces b and c). Similarly, the RR spectra of both ferric and ferrous $Mhcd_1$-NO adducts in solution are indicative of several co-existing spin configurations (Fig 6).
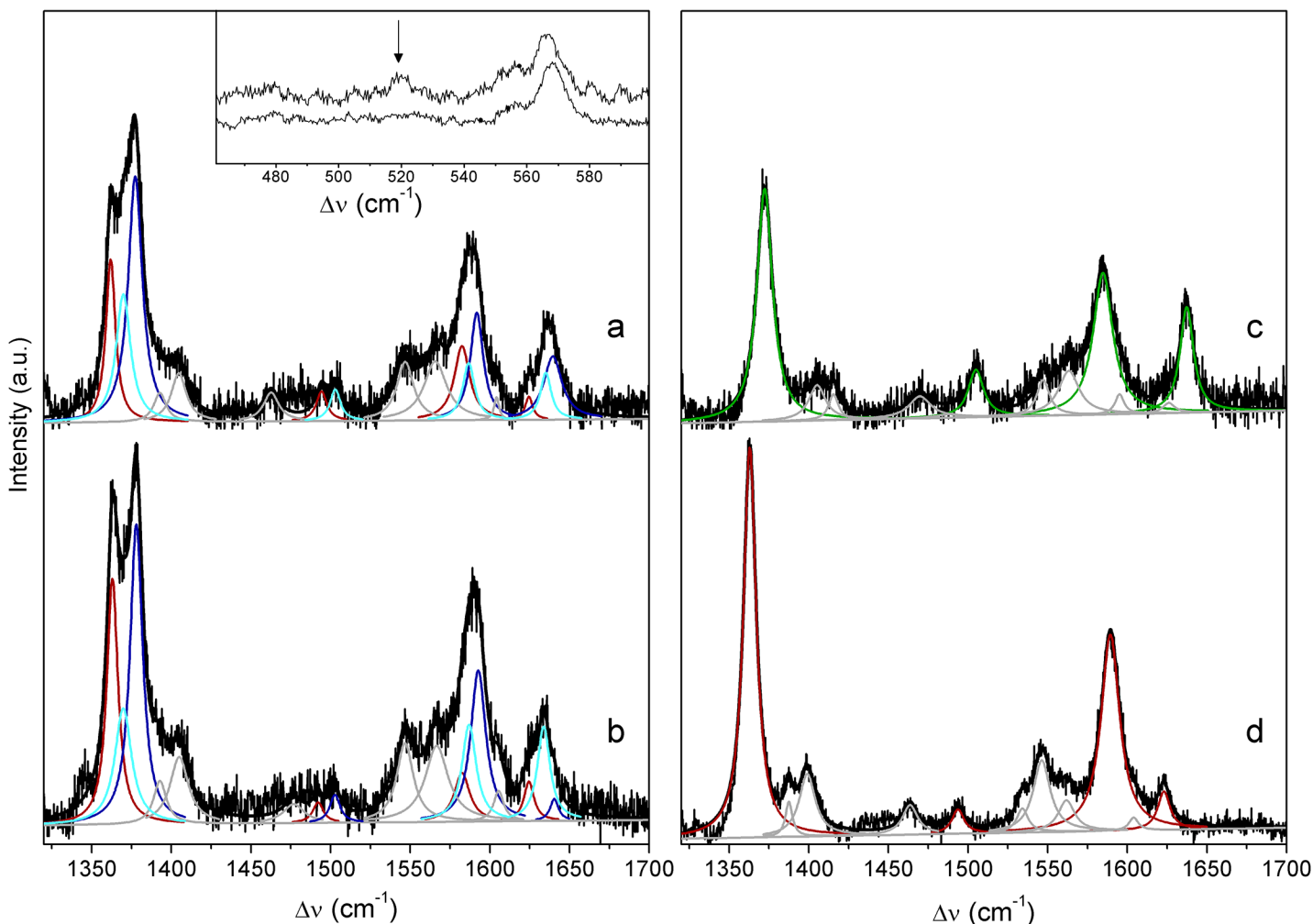
Fig 6. RR spectra of *Mhcd₁*-NO adducts and *Mhcd₁* prior to NO binding. (a) Ferric and (b) ferrous NO adducts of *Mhcd₁* measured upon addition of diethylamine NONOate; (c) ferric and (d) ferrous *Mhcd₁* prior to addition of NO. The spectra were measured with 413 nm excitation, 1.6 mW laser power and 40 s accumulation time. Component spectra represent ferrous population (red), 6cLS NO adduct (light blue), 5cHS NO adduct (blue), ferric population (green), non-assigned bands (gray) and overall fit (black). **Inset:** low frequency region of RR spectra of ferric *Mhcd₁*-NO adduct (top trace) and ferric *Mhcd₁* (bottom trace). The arrow designates the (d_1)Fe-NO stretching coordinate of 5c nitrosyl *Mhcd₁* complex.

doi:10.1371/journal.pone.0129940.g006

Due to the blue shift of the Soret band of heme d_1 upon NO binding, both hemes are probed with 413 nm excitation. Component analysis of the ferric-NO adduct (Fig 6, trace a) reveals a species with ν_4, ν_3, ν_2, and ν_{10} at 1362, 1494, 1582 cm^{-1}, and 1624 cm^{-1}, respectively. We attribute this species to the ferrous heme c (Fig 6A, red), which was also observed in the UV-Vis spectra (S3 Fig, trace b). We identified two additional species, a minor contribution with the corresponding marker bands at 1370, 1503, 1587, and 1635 cm^{-1} (Fig 6A, light blue), and the prevailing species, with the marker bands ν_4, ν_2, and ν_{10} at 1377, 1592, and 1640 cm^{-1} (Fig 6A, blue), respectively (cf. Table 1). These two species were not observed in the spectra of ferric (or ferrous) enzyme measured prior to addition of the NO donor (Fig 6, traces c and d). In analogy to other NO binding heme proteins, we attribute the minority species to the ferrous 6cLS NO adduct (i.e. c^{2+}/6cLS $d_1{}^{2+}$-NO), and the second species to the ferrous five-coordinated high spin (5cHS) NO adduct in which the proximal ligand of heme d_1 has been detached (i.e. c^{2+}/5cHS $d_1{}^{2+}$-NO) [39–41]. Nitric oxide is well-known as a strong trans-destabilizing ligand

that in its heme complexes can cause disruption of the bond between the heme iron and proximal His ligand, resulting in 5cHS Fe^{2+}-NO complex. The atypically high frequencies of the marker bands of NO adducts, also observed in model compounds and various NO binding heme proteins, have been attributed to a decrease in the electron density of the π^* antibonding orbitals of the porphyrin macrocycle by back-bonding to NO through the iron d_π orbitals [42,43]. Further evidence for the formation of a 5c nitrosyl $Mhcd_1$ complex comes from the low-frequency region (300 – 600 cm^{-1}) of the RR spectra, where an additional broad band appears at ~ 520 cm^{-1} in the presence of NO (Fig 6, inset upper trace). Despite of its very low intensity, this band is clearly absent in the spectra of the ferric protein. The frequency of the band falls into the 520 – 526 cm^{-1} range observed for the Fe-NO stretching in 5c-NO adducts of c-type cytochromes [39–42]. The 6cLS nitrosyl adducts of heme proteins tend to have a stronger Fe^{2+}-NO bond, with the stretching frequency in the range of 536 – 580 cm^{-1} [39,41], but due to a relatively low contribution of this species (Fig 6A, light blue), it could not be detected in the spectra of $Mhcd_1$. Actually, the 6cLS Fe^{2+}-NO stretching coordinate has been detected at very high frequency (~ 585 cm^{-1}) in $Pacd_1$-NO adduct, which has been rationalized in terms of the particular structural characteristics of the heme d_1 in comparison to other hemes [4]. The features of ferrous heme c, observed in UV-Vis and RR spectra of ferric $Mhcd_1$-NO mixture, have been previously reported for cd_1NiR-NO complexes from other organisms and were ascribed to auto-reduction [44–46]. We can hypothesize that cross-ET from heme d_1 to heme c can take place. In fact, a similar scenario was proposed for $Ppcd_1$, in which after nitrite reduction, an internal ET can occur from heme d_1^{2+}-NO to heme c^{3+}, resulting in ~ 45% of ferrous heme c present in solution, implying the formation of an approximately equimolar mixture of c^{2+}/d_1^{2+}-NO$^+$ and c^{3+}/d_1^{2+}-NO [47]. The component analysis of the ferrous-NO adduct of $Mhcd_1$ (Fig 6, trace b) reveals the same species described for the ferric complex.

Based on deconvoluted RR spectra of $Mhcd_1$-NO adducts, we demonstrate here that $Mhcd_1$ is capable of forming a NO-bound 5cHS state in which the proximal His is detached from the heme. A similar scenario was observed in NO binding and sensing proteins e.g. GSUs, CooA, sGC, etc [39–41], but formation of 5cHS NO adduct was not previously reported in cd_1NiRs. Despite the quite distinct RR fingerprint of $Mhcd_1$-NO complex, it could not be observed in SERR spectra of immobilized $Mhcd_1$, indicating that in neither of the tested conditions (vide infra) the enzyme was properly oriented for NO binding.

No further insights could be obtained from $Mhcd_1$ immobilized under different conditions and thus possibly alternative orientations. When $Mhcd_1$ was attached onto pure hydrophobic, OH/CH$_3$- or COO$^-$/CH$_3$- terminated SAMs, SERR signals were not stable, as exposure to potentials below 200 mV led to a signal loss after approximately 5 minutes. Additionally, the SERR signal intensity was ca. 3 times weaker on these SAMs in comparison with that on NH$_2^+$/CH$_3$ coated electrodes (vide supra). The protein could not be immobilized on pure hydroxyl-terminated SAMs, regardless of the immobilization conditions (e.g. "in-cell" or immersion of the electrode into concentrated protein solution externally; positive vs. negative electrode potentials vs. open circuit for "in-cell" immobilization; duration of the immobilization procedure or protein concentration; pH of the buffer; temperature; etc.), while the attempts to attach $Mhcd_1$ on carboxylate-, and pure amino-terminated SAMs resulted in weak or redox inactive signals.

In conclusion, we demonstrated in this work that among diverse alkanethiol-based SAMs which were tested for immobilization of $Mhcd_1$, only ´diluted´ positively charged surfaces (mixed NH$_2^+$/CH$_3$ monolayers) resulted in the attachment of a stable, redox active enzyme. The apparently structurally intact redox couple, associated with heme c, reveals ca. 150 mV negative shift of the redox potential in comparison with the solution value. Cyt c_{552}, on the other hand, preserves its structural and thermodynamic properties in the immobilized state.

Neither adsorbed $Mhcd_1$ nor cyt c_{552}/$Mhcd_1$ complexes assembled under different immobilization conditions were capable of nitrite reduction. Most likely, the altered redox properties, together with an orientation of the immobilized $Mhcd_1$ that is unfavorable for efficient heterogeneous ET and NO binding, are responsible for the lack of catalytic activity of the immobilized $Mhcd_1$. Clearly, very specific docking/orientation between $Mhcd_1$ and its redox partner needs to be achieved, as also demonstrated for e.g. CYPOR and CYP couple, for which both ET and allosteric modulation were found to be highly dependent on the intermolecular interaction [48]. Taken together, the present study reveals that the development of 3rd generation nitrite biosensor based on $Mhcd_1$ is not feasible at this point. Electrocatalysis of $Mhcd_1$ critically depends on interactions with its physiological electron donor.

Supporting Information

S1 Fig. Cyclic voltammograms of Au // 6-mercapto-1-hexanol /6-hexanethiol // cyt c_{552} // $Mhcd_1$ constructs. Cyclic voltammograms in the absence of nitrite (black line), and in the presence of 3 mM nitrite (red dashed line). Scan rate 50 mV/s. Supporting electrolyte: MES buffer 50 mM with 50 mM KCl, pH 6.3. The peaks correspond to the reversible electrochemical oxidation/reduction of cyt c_{552}.
(TIF)

S2 Fig. Scan rate dependence of the electrochemical response of cyt c_{552} immobilized on 6-mercapto-1-hexanol/6-hexanethiol coated Ag electrodes. A) Cyclic voltammograms at varying scan rates (0.01, 0.02, 0.035, 0.05, 0.075, 0.1, 0.2, 0.3 and 0.5 V/s). **B)** Variation of the anodic (squares) and cathodic (circles) peak currents of adsorbed cyt c_{552} as a function of the scan rate. Supporting electrolyte: 12.5 mM phosphate buffer and 12.5 mM K_2SO_4, pH 7.0.
(TIF)

S3 Fig. Electron absorption spectra of $Mhcd_1$. Ferric enzyme in the (a) absence and (b) presence of diethylamine NONOate and ferrous $Mhcd_1$ in the (c) presence and (d) absence of the NO donor. $Mhcd_1$ was 5 M in 50 mM Tris-HCl buffer, pH 7.6; protein was reduced with sodium ascorbate. Asterisk designates the Soret band of reduced heme d_1 (460 nm) and the arrow marks the 644 nm band indicative of NO binding to the ferric and ferrous enzyme.
(TIF)

Author Contributions

Conceived and designed the experiments: CMS POQ IM JJGM PH MGA ST. Performed the experiments: CMS POQ ST. Analyzed the data: CMS ST. Contributed reagents/materials/analysis tools: IM JJGM PH MGA ST. Wrote the paper: CMS PH MGA ST.

References

1. Cutruzzolà F. Bacterial nitric oxide synthesis. BBA. Bioenergetics. 1999; 1411: 231–249. PMID: 10320660

2. Cutruzzola F, Rinaldo S, Castiglione N, Giardina G, Pecht I, Brunori M. Nitrite reduction: a ubiquitous function from a pre-aerobic past. Bioessays. 2009; 31: 885–891. doi: 10.1002/bies.200800235 PMID: 19554608

3. Wherland S, Farver O, Pecht I. Intramolecular electron transfer in nitrite reductases. Chemphyschem. 2005; 6: 805–812. PMID: 15884062

4. Das TK, Wilson EK, Cutruzzola F, Brunori M, Rousseau DL. Binding of NO and CO to the d_1 Heme of cd_1 nitrite reductase from *Pseudomonas aeruginosa*. Biochemistry. 2001; 40: 10774–10781. PMID: 11535052

5. Nurizzo D, Cutruzzola F, Arese M, Bourgeois D, Brunori M, Cambillau C, et al. Conformational Changes Occurring upon Reduction and NO Binding in Nitrite Reductase from *Pseudomonas aeruginosa*. Biochemistry. 1998; 37: 13987–13996. PMID: 9760233

6. Nurizzo D, Cutruzzola F, Arese M, Bourgeois D, Brunori M, Cambillau C, et al. Does the reduction of *c* heme trigger the conformational change of crystalline nitrite reductase? J Biol Chem. 1999; 274: 14997–15004. PMID: 10329702

7. Nurizzo D, Silvestrini MC, Mathieu M, Cutruzzola F, Bourgeois D, Fulop V, et al. N-terminal arm exchange is observed in the 2.15 A crystal structure of oxidized nitrite reductase from *Pseudomonas aeruginosa*. Structure. 1997; 5: 1157–1171. PMID: 9331415

8. Farver O, Brunori M, Cutruzzola F, Rinaldo S, Wherland S, Pecht I. Intramolecular electron transfer in *Pseudomonas aeruginosa* cd_1 nitrite reductase: thermodynamics and kinetics. Biophys J. 2009; 96: 2849–2856. doi: 10.1016/j.bpj.2008.12.3937 PMID: 19348767

9. Rinaldo S, Arcovito A, Brunori M, Cutruzzola F. Fast dissociation of nitric oxide from ferrous *Pseudomonas aeruginosa* cd_1 nitrite reductase. A novel outlook on the catalytic mechanism. J Biol Chem. 2007; 282: 14761–14767. PMID: 17389587

10. Rinaldo S, Brunori M, Cutruzzolà F. Nitrite controls the release of nitric oxide in *Pseudomonas aeruginosa* cd_1 nitrite reductase. Biochem Biophys Res Commun. 2007; 363: 662–666. PMID: 17904106

11. Rinaldo S, Sam KA, Castiglione N, Stelitano V, Arcovito A, Brunori M, et al. Observation of fast release of NO from ferrous d haem allows formulation of a unified reaction mechanism for cytochrome cd_1 nitrite reductases. Biochem J. 2011; 435: 217–225. doi: 10.1042/BJ20101615 PMID: 21244362

12. Williams PA, Fulop V, Garman EF, Saunders NF, Ferguson SJ, Hajdu J. Haem-ligand switching during catalysis in crystals of a nitrogen-cycle enzyme. Nature. 1997; 389: 406–412. PMID: 9311786

13. Almeida MG, Serra A, Silveira CM, Moura JJG. Nitrite Biosensing via Selective Enzymes-A Long but Promising Route. Sensors. 2010; 10: 11530–11555. doi: 10.3390/s101211530 PMID: 22163541

14. Rosa CC, Cruz HJ, Vidal M, Oliva AG. Optical biosensor based on nitrite reductase immobilized in controlled pore glass. Biosens Bioelectron. 2002; 17: 45–52. PMID: 11742734

15. Noll T, Noll G. Strategies for "wiring" redox-active proteins to electrodes and applications in biosensors, biofuel cells, and nanotechnology. Chem Soc Rev. 2011; 40: 3564–3576. doi: 10.1039/c1cs15030h PMID: 21509355

16. Willner B, Katz E, Willner I. Electrical contacting of redox proteins by nanotechnological means. Curr Opin Biotechnol. 2006; 17: 589–596. PMID: 17084610

17. Sezer M, Millo D, Weidinger IM, Zebger I, Hildebrandt P. Analyzing the catalytic processes of immobilized redox enzymes by vibrational spectroscopies. IUBMB Life. 2012; 64: 455–464. doi: 10.1002/iub.1020 PMID: 22535701

18. Ash PA, Vincent KA. Spectroscopic analysis of immobilised redox enzymes under direct electrochemical control. Chem Commun. 2012; 48: 1400–1409. doi: 10.1039/c1cc15871f PMID: 22057715

19. Murgida DH, Hildebrandt P. Electron-Transfer Processes of Cytochrome *c* at Interfaces. New Insights by Surface-Enhanced Resonance Raman Spectroscopy. Acc Chem Res. 2004; 37: 854–861. PMID: 15612675

20. Todorovic S, Jung C, Hildebrandt P, Murgida DH. Conformational transitions and redox potential shifts of cytochrome P450 induced by immobilization. J Biol Inorg Chem. 2006; 11: 119–127. PMID: 16328458

21. Todorovic S, Verissimo A, Wisitruangsakul N, Zebger I, Hildebrandt P, Pereira MM, et al. SERR-Spectroelectrochemical Study of a cbb$_3$ Oxygen Reductase in a Biomimetic Construct. J Phys Chem B. 2008; 112: 16952–16959. doi: 10.1021/jp807862m PMID: 19053671

22. Lojou E, Cutruzzolà F, Tegoni M, Bianco P. Electrochemical study of the intermolecular electron transfer to *Pseudomonas aeruginosa* cytochrome cd_1 nitrite reductase. Electrochim Acta. 2003; 48: 1055–1064.

23. Lopes H, Besson S, Moura I, Moura JJ. Kinetics of inter- and intramolecular electron transfer of *Pseudomonas nautica* cytochrome cd_1 nitrite reductase: regulation of the NO-bound end product. J Biol Inorg Chem. 2001; 6: 55–62. PMID: 11191223

24. Serra AS, Jorge SR, Silveira CM, Moura JJ, Jubete E, Ochoteco E, et al. Cooperative use of cytochrome cd_1 nitrite reductase and its redox partner cytochrome c_{552} to improve the selectivity of nitrite biosensing. Anal Chim Acta. 2011; 693: 41–46. doi: 10.1016/j.aca.2011.03.029 PMID: 21504809

25. Serra A. Isolamento e Caracterização de Enzimas Multihémicas de Origem Microbiana e sua Aplicação no Desenvolvimento de Biossensores. PhD Thesis, Universidade Nova de Lisboa. 2012. Available: http://hdl.handle.net/10362/7627.

26. Besson S, Carneiro C, Moura JJ, Moura I, Fauque G. A cytochrome cd_1-type nitrite reductase isolated from the marine denitrifier *Pseudomonas nautica* 617: purification and characterization. Anaerobe. 1995; 1: 219–226. PMID: 16887530

27. Fauque G, Moura JJG, Besson S, Saraiva L, Moura I. Preliminary characterization of the cytochrome system in the marine denitrifying bacterium *Pseudomonas nautica* 617. Oceanis. 1992; 18: 211–216. PMID: 1449420

28. Murgida DH, Hildebrandt P. Heterogeneous Electron Transfer of Cytochrome *c* on Coated Silver Electrodes. Electric Field Effects on Structure and Redox Potential. J Phys Chem B. 2001; 105: 1578–1586.

29. Döpner S, Hildebrandt P, Grant Mauk A, Lenk H, Stempfle W. Analysis of vibrational spectra of multicomponent systems. Application to pH-dependent resonance Raman spectra of ferricytochrome *c*. Spectrochim Acta A Mol Biomol Spectrosc. 1996; 52: 573–584.

30. Saraiva LM, Fauque G, Besson S, Moura I. Physico-chemical and spectroscopic properties of the monohemic cytochrome C_{552} from *Pseudomonas nautica* 617. Eur J Biochem. 1994; 224: 1011–1017. PMID: 7925398

31. Brown K, Nurizzo D, Besson S, Shepard W, Moura J, Moura I, et al. MAD structure of *Pseudomonas nautica* dimeric cytochrome c_{552} mimicks the c_4 dihemic cytochrome domain association. J Mol Biol. 1999; 289: 1017–1028. PMID: 10369779

32. Sun Y, Benabbas A, Zeng W, Kleingardner JG, Bren KL, Champion PM. Investigations of heme distortion, low-frequency vibrational excitations, and electron transfer in cytochrome *c*. Proc Natl Acad Sci U S A. 2014; 111: 6570–6575. doi: 10.1073/pnas.1322274111 PMID: 24753591

33. Ching Y, Ondrias MR, Rousseau DL, Muhoberac BB, Wharton DC. Resonance Raman spectra of heme *c* and heme d_1 in *Pseudomonas* cytochrome oxidase. FEBS Lett. 1982; 138: 239–244. PMID: 6279445

34. Latypov RF, Maki K, Cheng H, Luck SD, Roder H. Folding Mechanism of Reduced Cytochrome *c*: Equilibrium and Kinetic Properties in the Presence of Carbon Monoxide. J Mol Biol. 2008; 383: 437–453. doi: 10.1016/j.jmb.2008.08.025 PMID: 18761351

35. Santos H, Turner DL. Characterization and NMR studies of a novel cytochrome *c* isolated from *Methylophilus methylotrophus* which shows a redox-linked change of spin state. BBA. Protein structure and molecular enzymology. 1988; 954: 277–286.

36. Koppenhofer A, Turner KL, Allen JW, Chapman SK, Ferguson SJ. Cytochrome cd_1 from *Paracoccus pantotrophus* exhibits kinetically gated, conformationally dependent, highly cooperative two-electron redox behavior. Biochemistry. 2000; 39: 4243–4249. PMID: 10757972

37. Silvestrini MC, Tordi MG, Colosimo A, Antonini E, Brunori M. The kinetics of electron transfer between *Pseudomonas aeruginosa* cytochrome *c*-551 and its oxidase. Biochem J. 1982; 203: 445–451. PMID: 6288000

38. Kassner RJ. Theoretical model for the effects of local nonpolar heme environments on the redox potentials in cytochromes. J Am Chem Soc. 1973; 95: 2674–2677. PMID: 4348492

39. Andrew CR, George SJ, Lawson DM, Eady RR. Six- to five-coordinate heme-nitrosyl conversion in cytochrome *c'* and its relevance to guanylate cyclase. Biochemistry. 2002; 41: 2353–2360. PMID: 11841228

40. Andrew CR, Green EL, Lawson DM, Eady RR. Resonance Raman studies of cytochrome *c'* support the binding of NO and CO to opposite sides of the heme: implications for ligand discrimination in heme-based sensors. Biochemistry. 2001; 40: 4115–4122. PMID: 11300792

41. Reynolds MF, Parks RB, Burstyn JN, Shelver D, Thorsteinsson MV, Kerby RL, et al. Electronic absorption, EPR, and resonance raman spectroscopy of CooA, a CO-sensing transcription activator from R. rubrum, reveals a five-coordinate NO-heme. Biochemistry. 2000; 39: 388–396. PMID: 10631000

42. Quintas PO, Catarino T, Todorovic S, Turner DL. Highly selective ligand binding by *Methylophilus methylotrophus* cytochrome *c''*. Biochemistry. 2011; 50: 5624–5632. doi: 10.1021/bi200480a PMID: 21599015

43. Soldatova AV, Ibrahim M, Olson JS, Czernuszewicz RS, Spiro TG. New Light on NO Bonding in Fe(III) Heme Proteins from Resonance Raman Spectroscopy and DFT Modeling. J Am Chem Soc. 2010; 132: 4614–4625. doi: 10.1021/ja906233m PMID: 20218710

44. Shimada H, Orii Y. The nitric oxide compounds of *Pseudomonas aeruginosa* nitrite reductase and their probable participation in the nitrite reduction. FEBS Lett. 1975; 54: 237–240. PMID: 805716

45. Silvestrini MC, Colosimo A, Brunori M, Walsh TA, Barber D, Greenwood C. A re-evaluation of some basic structural and functional properties of *Pseudomonas* cytochrome oxidase. Biochem J. 1979; 183: 701–709. PMID: 44192

46. Wang Y, Averill BA. Direct Observation by FTIR Spectroscopy of the Ferrous Heme–NO$^+$ Intermediate in Reduction of Nitrite by a Dissimilatory Heme cd_1 Nitrite Reductase. J Am Chem Soc. 1996; 118: 3972–3973.

47. George SJ, Allen JW, Ferguson SJ, Thorneley RN. Time-resolved infrared spectroscopy reveals a stable ferric heme-NO intermediate in the reaction of *Paracoccus pantotrophus* cytochrome cd_1 nitrite reductase with nitrite. J Biol Chem. 2000; 275: 33231–33237. PMID: 10922371

48. Aigrain L, Pompon D, Morera S, Truan G. Structure of the open conformation of a functional chimeric NADPH cytochrome P450 reductase. EMBO Rep. 2009; 10: 742–747. doi: 10.1038/embor.2009.82 PMID: 19483672